Chapter V

Schiff Base Triggering Synthesis of Copper(II) Complex and its Catalytic Fate towards Mimics of Phenoxazinone Synthase Activity

5.1. Introduction

Copper based coordination compounds containing Schiff base ligands have been widely employed in different organic transformations of laboratory and industrial significance.[1-3] In living system, copper ion has played a pivotal role as an essential bio-element. In addition, copper complexes have been widely distributed as the functional sites of various metal dependent enzymes like catechol and galactose oxidase, phenoxazinone synthase, superoxide dismutase, lysine oxidase, N_2O reductase etc.[4-7] Enormous efforts have been made by renowned research groups to mimic structural and functional sites of copper dependent enzymes aiming to develop better catalysts by tuning the electronic and geometric factors associated with the surrounding ligands.[8-10] It has commonly been observed that proper tuning of electronic and steric factors in ligand may lead to improve molecular properties for metal complexes.[4-11]

Among the copper(II) complexes of varied nuclearities, dicopper compounds have played significant role in mimicking the functional activities of type-3 copper proteins with high efficiency.[4-7] Focusing on those structural and functional aspects, synthetic inorganic chemists have actively engrossed in designing and synthesizing coordination compounds aiming to explore the bio-functions of various metal-dependent enzymes.[11] Type-3 copper proteins have a dinuclear copper(II) active site and both the copper(II) centers were antiferromagnetically coupled that makes them EPR silent.[12-14] The magnetic interactions involving phenoxo-bridged complex **4** have been widely investigated in the scientific literature.[15-21] There were lots of examples where dinuclear copper complexes have formed by bridging phenolates and other atomic or molecular bridges (oxides, pyrazoles, phosphates, acetates etc).[22-29]

On the other hand, catalytic oxidative coupling from 2-aminophenol (2-AP) to 2-amino-3H-phenoxazine-3-one (2-APX) by copper(II) based coordination compounds have drawn considerable attention for its important mechanistic insights in the course of oxidative catalysis.[30-37] It has been experimentally observed that a naturally occurring antineoplastic agent, actinomycin D behaves as an inhibitor towards the preparation of DNA-directed RNA. Actinomycin D was related to questiomycin A which was familiar

as 2-Amino-3H-phenoxazine-3-one.[38] This species was used clinically for the treatment of certain types of cancer.[39] It was well observed that in the final step of the biosynthesis of actinomycin D, the enzyme phenoxazinone synthase catalyzes the oxidative coupling of 2-aminophenol to the phenoxazinone chromophore.[39-41] On account of the significance of the oxidative catalysis, this research work presented the preparation, structural characterization and DFT study of a dinuclear copper(II)-Schiff base complex and its potential bio-mimicking activity towards catalytic oxidative coupling of 2-aminophenol under aerobic atmosphere. [**L^4**= (Z)-2-methoxy-6-(((2-methoxyphenyl)imino) methyl)phenol), **Scheme 5.1**]

Scheme 5.1. Schematic diagram of the ligand **L^4**

5.2. Experimental Section

5.2.1. Preparation of the complex

5.2.1.1. Materials and Methods

Highly pure *o*-vanilin (Sigma Aldrich, USA), *o*-anisidine (Sigma Aldrich, USA), copper(II) perchlorate hexahydrate (E-Merck, India) and *o*-aminophenol (Sigma Aldrich, USA) were purchased from the respective concerns and used as received. All other chemicals and solvents were of analytical grade and were used as received without further purification.

Caution! Metal perchlorate salts are potentially explosive, especially in presence of organic ligands. Hence, metal perchlorate salts should only be handled with proper precautions (in small amount, avoid heat and fire).

5.2.1.2. Synthesis of the Schiff base L^4 and copper complex 4

The Schiff base ligand, **L^4** was prepared following the reported procedure.[42-44] The Schiff base ligand was synthesised by refluxing *o*-anisidine (0.123 g, 1 mmol) with *o*-vanilin (0.152 g, 1 mmol) in 20 ml ethanol for 6 h. Thereafter, the reddish coloured solution was filtered and dried. Then, the compound was stored in vaccuo over $CaCl_2$ for use. The Cu complex **4** was synthesized in methanolic solution of $Cu(ClO_4)_2$ (0.730

g, 2 mmol) was added drop wise to the acetonitrile solution of **L**^{4} (0.771 g, 3 mmol). Consequently, it was observed that the red coloured Schiff base solution was turned into green immediately. The, the reaction solution was kept in open atmosphere for slow evaporation. After 10-15 days, fine microcrystalline green coloured compound was separated out from the solution. Thereafter, the crystalline compound was washed with toluene and dried over silica gel to get pure crystals of **4**. Finally, different spectroscopic and analytical techniques were performed to characterize the compound. The results are as follows.

Yield of **L**^{4}: 0.219 g (~85.2%).

Yield of **4**: 0.630 g (~76% based on metal salt).

5.2.2. Physical measurements

IR spectra of the ligand **L**^{4} and **4** were recorded with a FTIR-8400S SHIMADZU spectrophotometer (Shimadzu, Kyoto, Japan) in the range 400-3600 cm^{-1} with KBr pellet. ^{1}H and ^{13}C NMR spectra of the ligand (**L**^{4}) were recorded on a Bruker Advance 400 MHz spectrometer (Bruker, Massachusetts, USA) in $CDCl_3$ at 298 K. Steady-state absorption and other spectral data were recorded with a JASCO V-730 UV-Vis spectrophotometer (Jasco, Tokyo, Japan). Electrospray ionization (ESI) mass spectrum of the ligand and **4** were recorded using a Q-tof-micro quadruple mass spectrometer. Operating parameters of the instrument like sample cone, source temperature, and pump flow were kept as fixed at 30V, 80 ºC and 20 µL/min respectively during the measurement of ESI-MS for this dicopper(II) complex. The pH values of different solutions were measured by Labman pH meter (Wensar, Chennai, India) at room temperature. Elemental analyses were performed on a Perkin Elmer 2400 CHN microanalyser (Perkin Elmer, Waltham, USA). X-band EPR spectra were recorded on a Magnettech GmbH MiniScope MS400 spectrometer (equipped with temperature controller TC H03, Magnettech, Berlin, Germany), where the microwave frequency was measured with an FC400 frequency counter.

Table 5.1. CHN analysis of the Schiff base ligand **L**^{4} and complex **4**

Compound (Mol. formula)	**Found (Calcd)%**		
	C	**H**	**N**
L^{4} ($C_{15}H_{15}NO_3$)	70.09 (70.02)	5.80 (5.88)	5.93 (5.44)

Complex 4 ($C_{45}H_{42}N_3O_{13}ClCu_2$)	54.35 (54.30)	4.19 (4.25)	4.28 (4.22)

5.2.3. Crystal structure determination and refinement

Single crystal X-ray diffraction data of **4** were collected using a Rigaku XtaLABmini diffractometer equipped with Mercury 375R (2 × 2 bin mode) CCD detector. The data were collected with graphite monochromated Mo-Kα radiation (λ=0.71073 Å) at 100.0(2) K using ω scans. The data were reduced using CrysAlisPro 1.171.38.46[45] and the space group determination was done using Olex2. The structure was resolved by dual space method using SHELXT-2015[46] and refined by full-matrix least-squares procedures using the SHELXL-2015 [47] software package through OLEX2 suite.[48]

5.2.4. Hirshfeld surface analysis of complex 4

Crystal Explorer 17.5[49] progam package was employed to generate Hirshfeld surfaces [50] and 2D fingerprint plots [51] of **4** using its single crystal X-ray diffraction data. It has already been established that Hirshfeld Surface analysis was a very important tool to study and locate intermolecular interactions within a crystal packing.[51,52] The function d_{norm} was a ratio of the distances of any surface point to the nearest interior (d_i) and exterior (d_e) atom and the van der Waals radii of the atoms.[53-55] The normalized contact distance (d_{norm}) could be expressed as

$$d_{norm} = \frac{d_i - r_i^{vdW}}{r_i^{vdW}} + \frac{d_e - r_e^{vdW}}{r_e^{vdW}} \qquad \text{...(5.1)}$$

Where, r_e^{vdW} and r_i^{vdW} denote the corresponding van der Waals radii of atoms. The negative value of d_{norm} indicates that the sum of d_i and d_e was shorter than the sum of the relevant van der Waals radii, which was considered to be a closest contact and was visualized in red colour. The white colour denotes intermolecular distances close to van der Waals contacts with d_{norm} equal to zero whereas contacts longer than the sum of van der Waals radii with positive d_{norm} values were coloured with blue. A plot of d_i versus d_e was a fingerprint plot that identifies the presence of different types of intermolecular interactions.

5.2.5. Phenoxazinone synthase activity of complex 4

Phenoxazinone Synthase like activity was examined by treating 1×10^{-4} M solution of **4** in MeCN medium with 10 equiv. of 2-aminophenol (2-AP) under aerobic conditions at

room temperature. To study this activity, absorbance vs. wavelength (wavelength scans) of the solution was monitored spectrophometrically at a regular time interval of 5 minutes for 1h in the wavelength range from 300-800 nm.[6,32,42]

Kinetic experiments were also performed spectrophotometrically to enumerate the aminophenol oxidation efficacy with this complex **4** in presence of 2-AP in MeCN at 298 K.[6,32,42] 0.04 mL of the complex solution with a constant concentration of 1×10^{-4} M was added to 2 mL of 2-AP of a particular concentration (varying its concentration from 1×10^{-3} M to 1×10^{-2} M) to achieve the ultimate concentration of the complex as 1×10^{-4} M. The conversion of 2-aminophenol to 2-aminophenoxazine-3-one was monitored with time at a wavelength 434 nm (time scan) in MeCN.[6,32,42,56-59] To determine the dependence of rate on substrate concentration, kinetic analyses were performed in triplicate.

Column chromatography was employed to extract the product, phenoxazinone in pure form from the catalytic oxidation of 2-AP. Neutral alumina was used as column support and benzene-ethyl acetate solvent mixture was treated as an eluant mixture in this chromatographic separation. The oxidation product was found in high yield (~77% for **4**). ^{1}H NMR spectral analysis helped to identify the species. ^{1}H NMR data for 2-amino-3*H*-phenoxazine-3-one (APX), ($CDCl_3$, 400 MHz,) δ_H: 7.62 (m, 1H), 7.44 (m, 3H), 6.47 (s, 1H), 6.39 (s, 1H), 6.28 (s, 1H). The identification of this phenoxazinone product was further consolidated in ESI-Ms spectrometry from the appearance of base peak at m/z 213.

5.2.6. Detection of presence of hydrogen peroxide in the catalytic oxidation of 2-aminophenol

To ensure the active participation of molecular oxygen in the course of catalysis, the formation of hydrogen peroxide was checked based on some previously reported literatures.[56-59] It was well known that molecular oxygen in oxidative catalytic reactions may convert itself to hydrogen peroxide or water as byproduct. In this course of oxidative catalytic reaction, the solution was acidified with H_2SO_4 to reach the pH of the solution at 2. After a certain time, an equal volume of water was added to stop further oxidation. The phenoxazinone species were extracted three times with dichloromethane. 1 mL of 10 % solution of KI and three drops of a 3 % solution of ammonium molybdate were added to the aqueous layer. The formation of I_3^- was

monitored spectrophotometrically to check the development of the characteristic I_3^- band (λ_{max}= 353 nm) which is assignable to the production of hydrogen peroxide.

5.2.7. Electro-chemical analysis

The electro analytical instrument, BASi Epsilon-EC for cyclic voltammetric experiment in CH_2Cl_2 solutions containing 0.2 M tetrabutylammonium hexafluorophosphate as supporting electrolyte was used. The BASi platinum working electrode, platinum auxiliary electrode, Ag/AgCl reference electrode were used for the measurements.

5.2.8. Computational details

All the computational calculations were performed using Gaussian 09 W Programme Suite[60] avoiding symmetrical restrictions. Employing density functional theory (DFT), all the ground state calculations were performed with widely used B3LYP computational model and 6-311G basis set (for both metal and non-metallic elements).[61] Initially, complex **4** was optimized in vacuum. Thereafter, to incorporate solvent effect, **4** was optimized in MeCN (ε = 35.668) employing integral equation formalism polar continuum model (IEFPCM).[62-65] solvent model. Global minimum of each structure was confirmed through stability calculations and IR frequency check-up with no imaginary frequency. All the optimized structures were stable under the perturbation considered. The images of frontier molecular orbitals (FMOs) were extracted from corresponding check point files. For further details of computational methods, readers might follow somewhere else.[66-68] To compare the XRD structure and computationally optimized structure visually, the structures were superimposed using PyMOL 1.3 software package.[70]

5.3. Results and discussion

5.3.1. Synthesis and formulation of the Schiff base L^4 and complex 4

The reddish coloured Schiff base ligand, $\mathbf{L^4}$ was synthesized by refluxing *o*-anisidine with o-vanillin in ethanol medium. Single crystals of the Schiff base were grown in the saturated solution of Schiff base in ethanol medium using slow evaporation technique (**Scheme 5.2**). The Schiff base exhibited good solubility in methanol, ethanol, and dimethylsulphoxide. The synthesis of the complex **4** were obtained by adding hydrated copper(II) perchlorate to polydentate Schiff base ligand (**Scheme 5.2**). Different ratio between hydrated $Cu(ClO_4)_2$ and $\mathbf{L^4}$ (1:1, 1:2) have also been applied to prepared the

single crystals to divulge the mode of coordination of the Schiff base with Cu(II) ion. However, no crystals were found. Different Cu(II) salts like bromide, acetate and sulphate have been combined with the polydentate Sciff base to prepare Cu(II) complexes of varied dimension and nuclearities but remains unsuccessful. This copper compound showed good solubility in common polar solvents as such methanol, acetonitrile, dichloromethane etc. This synthesis may be successfully prepared using methanol-dichloromethane or methanol-acetonitrile medium.

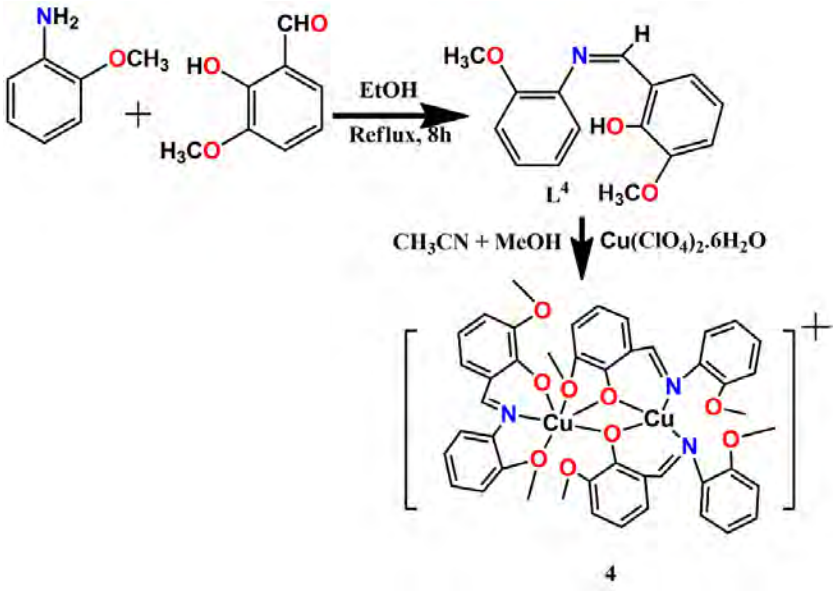

Scheme 5.2. Synthetic route for the complex **4**

5.3.2. Infrared spectral analysis

The Schiff base **L**^{4} ligand exhibited the characteristic peaks at 3432 and 1614 cm^{-1} for hydroxyl and imine groups respectively. The complex **4** showed the characteristic peaks at 1611 and 1095 cm^{-1} for methylene and perchlorate groups respectively. These characteristic peak of the Schiff base **L**^{4} ligand and complex **4** were tabulated in the given below **Table 5.2**.

Table 5.2. Infrared spectral data[a] of **L**^{4} **and 4**

Compounds	**ν (cm^{-1})**	**Functional groups**
L^{4}	3432 1614	–OH, –C=N–
Complex 4	1095, 1611	–ClO4^{-}, –C=N–

[a]KBr disc

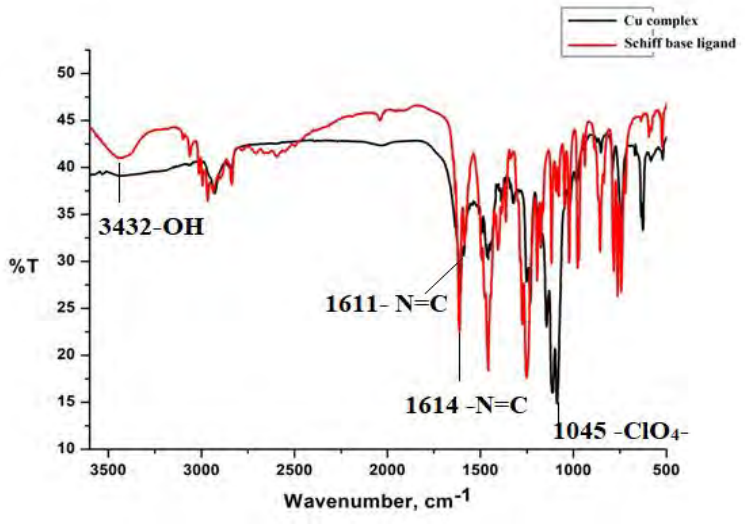

Fig. 5.1. FT-IR spectrum of the Schiff base **L**^{4} and complex **4**

5.3.3. Electronic spectral analysis

The electronic spectra of the **L**^{4} and complex **4** were recorded in acetonitrile medium (MeCN) from 200 to 900 nm at room temperature. The Schiff base, **L**^{4} displayed high intensity electronic bands at 278, 340 nm and a broad band at 460 nm while the complex **4** exhibited electronic transitions at 240, 293 and 400 nm. The optical bands for **L**^{4} & **4** were displayed in **Fig. 5.2**. The highly intense electronic bands at 278, 340 nm in UV region for **L**^{4} are assignable to π→π* and n→π* electronic transitions of ligand chromophore, however the development of optical band at 460 nm is assignable for charge transition of ligand origin.[71] The $^3A_{2g}(F) \rightarrow {}^3T_{2g}(F)$ transition that commonly appears above 700 nm was missing for this copper complex **4**.[72-74] The absorption at 400 nm corresponds to charge transfer transition and can be assignable to phenoxo to Cu(II) ion electron transfer transition.[73,74] The highly intense electronic bands at 240 and 293 nm for **4** may be attributed to π→π* and n→π* electronic transitions of ligand chromophore.[71]

Table 5.3. UV-Vis spectral data[b] of **L**^{4} **and 4**

Compounds	**λ_{max}, nm**
L^4	278 (0.21), 340 (0.28), 460 (0.09)
Complex 4	240 (0.78), 293(0.44), 400 (0.18)

[b]Acetonitrile solution in 298K

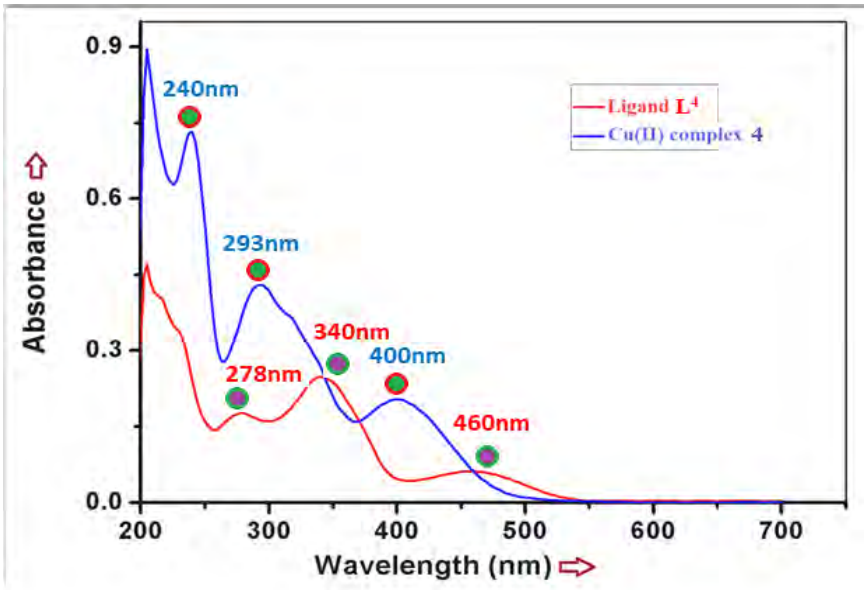

Fig.5.2. UV-Vis spectrum of the Schiff base $\mathbf{L^4}$ and complex **4** in MeCN medium

5.3.4. Fluorescence property

The fluorescence behaviour of the ligand and the complex **4** has been examined through recording of fluorescence spectra in MeCN medium & are presented in **Fig.5.3**. The Schiff base exhibited moderate intensity in fluorescence behaviour while complex **4** behaves as a non-fluorescent or poorly fluorescent compound at room temperature. The quenching of fluorescence intensity for Schiff base upon coordination of Cu(II) ion may be explained in terms of spin-orbit coupling or heavy atom effect.[76-78] Previously, Rathod *et al*, reported the similar kind of reduction of fluorescent intensity for highly fluorescent fluorescein-based Schiff base upon incorporation of Cu^{2+} ion in solution phase.[77]

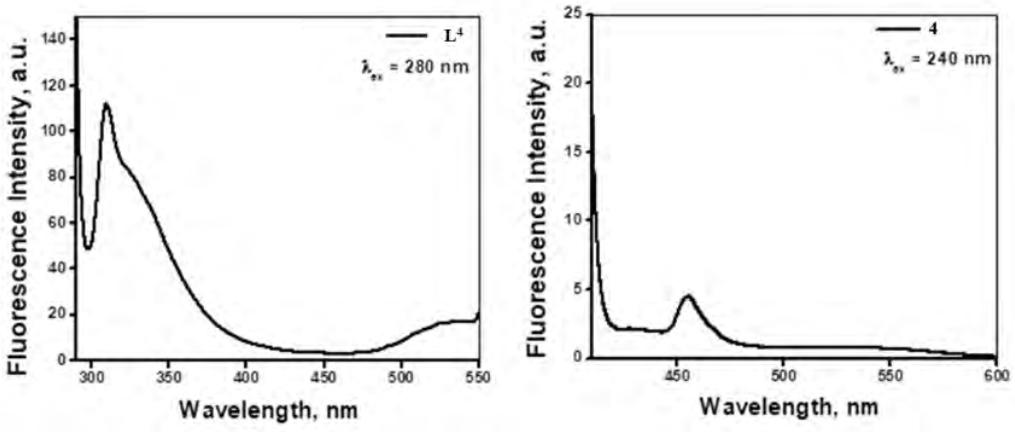

Fig.5.3. Steady-state fluorescence spectra of $\mathbf{L^4}$ (left) & complex **4** (right) in MeCN

5.3.5. Molar conductance measurement

The electrolytic nature of the complex **4** has also been examined through recording molar conductance values in MeCN medium at room temperature. The molar conductance values for 1.50×10^{-3} M concentration solution of **4** produces 147 Scm^2mol^{-1} which certainly recommends the 1:1 electrolytic nature in MeCN medium. The electrolytic nature of **4** was attributed for the existence cationic dicopper(II) species with counter anionic perchlorate ion.[75]

5.3.6. NMR spectral analysis

The NMR spectral analysis of $\mathbf{L^4}$ was carried out in $CDCl_3$. **Fig. 5.4** and **5.5** displayed the ^1H and ^{13}C NMR spectra of $\mathbf{L^4}$, respectively. The $\mathbf{L^4}$ ligand characteristic peak showed at 14.47 ppm for hydroxyl proton and 8.72 ppm assigning the methylene containing proton. The proton signals corresponding to aromatic-H appeared in the range 7.27 to 6.98 ppm while the -OCH_3 protons showed at 3.94 to 3.90 ppm.

The ^{13}C NMR was also recorded to assign the characteristics of the C-atom in $\mathbf{L^4}$. The signals exhibited at 161.33 ppm attributed the azomethine-C. The ph-C bound to -OMe and ph-C bound to -OH were attributed at 153.87, 152.68 and 148.77 ppm, respectively while the signals in the range 136.31 to 111.97 ppm corresponded to the aromatic-Cs and OCH_3 carbons showed at 56.12 to 55.85 ppm respectively in the $\mathbf{L^4}$.

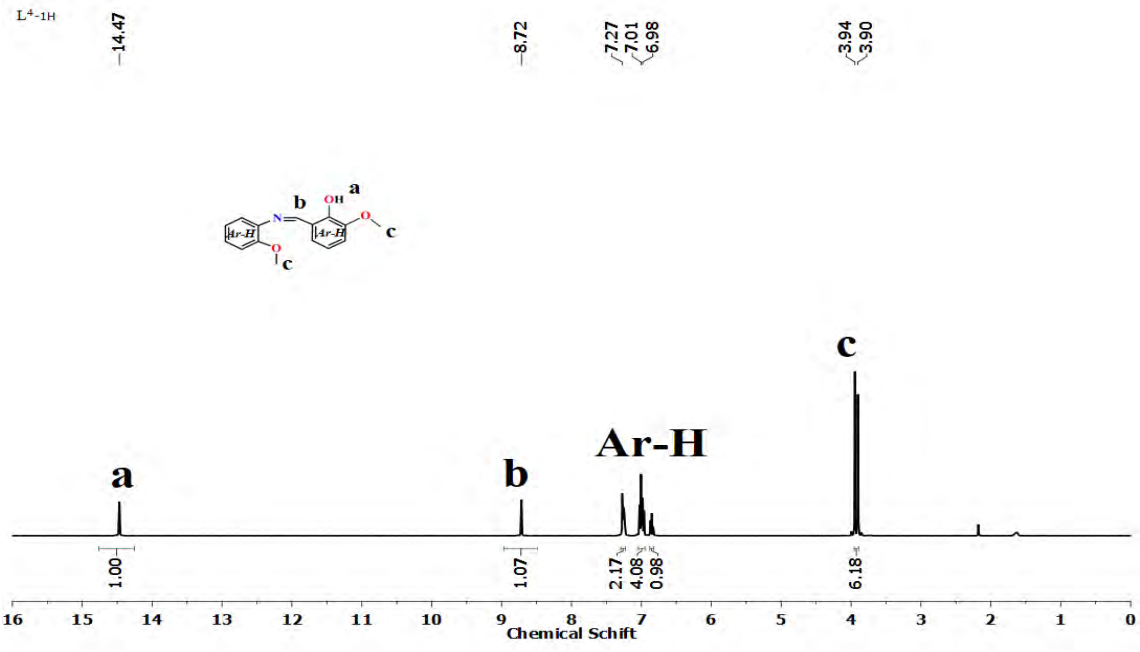

Fig. 5.4. ^1H NMR spectrum of the ligand, $\mathbf{L^4}$ in $CDCl_3$

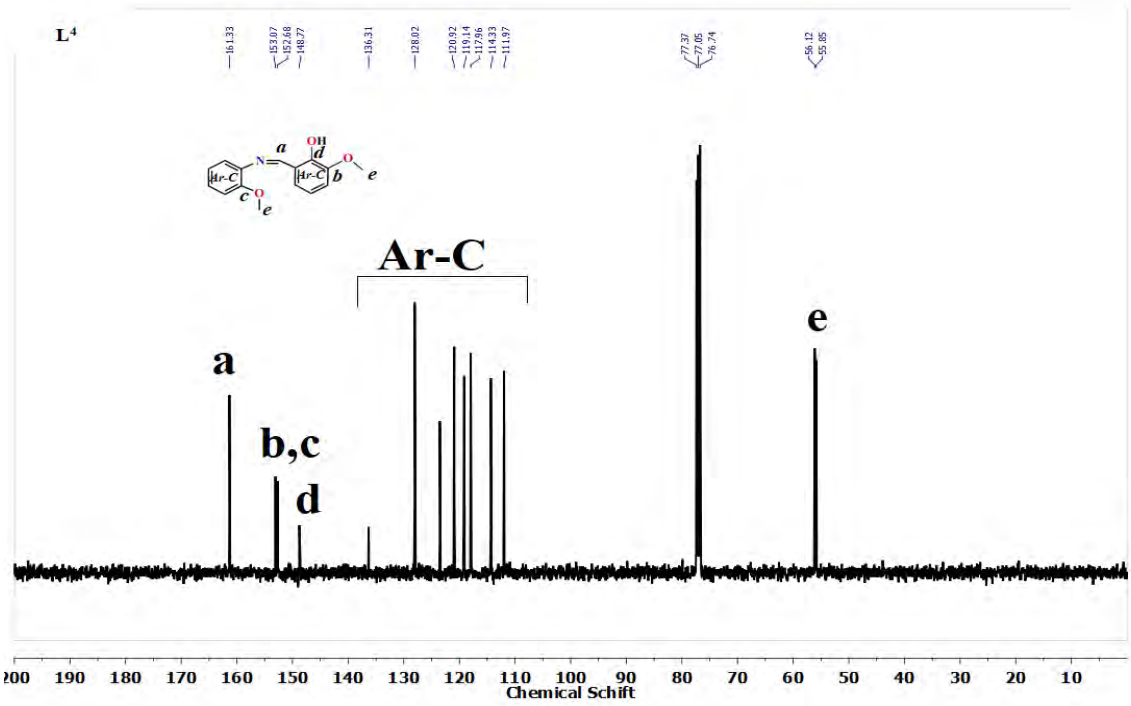

Fig. 5.5. ^{13}C NMR spectrum of the ligand, **L^4** in $CDCl_3$

5.3.7. ESI-Ms spectra analysis

ESI-Ms spectra of **L^4** and its Cu(II) compound were also measured in MeCN medium and the spectra were presented in **Fig.5.6 and 5.7**. Presence of molecular ion peaks at m/z 258.6663 (257.11) and 894.2371 (894.15) for **L^4** and **4** justify the molecular integrity of the compounds in solution phase. The experimental m/z values agree very well with the calculated values of molecular mass for both the compounds.

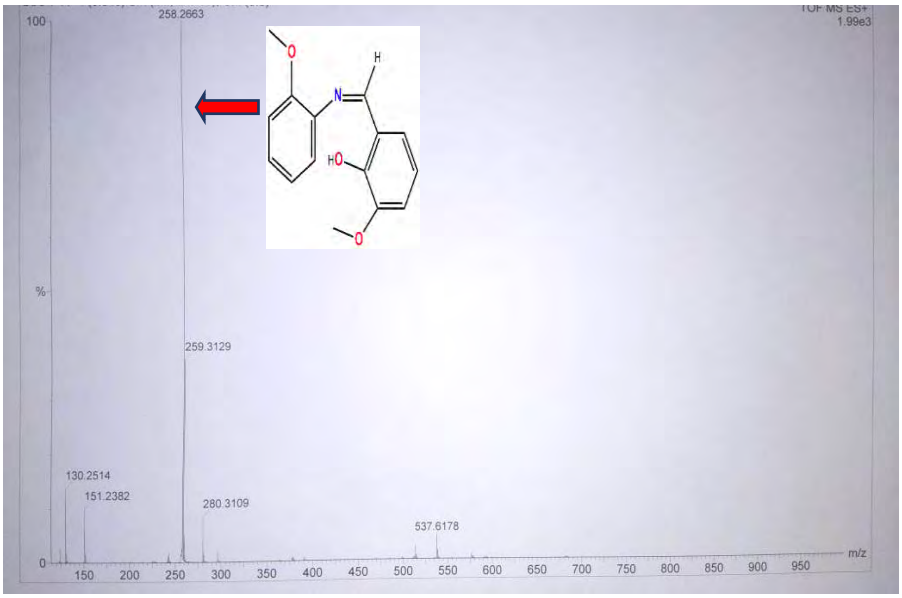

Fig. 5.6. ESI-Ms spectrum of the Schiff base **L^4** in MeCN medium

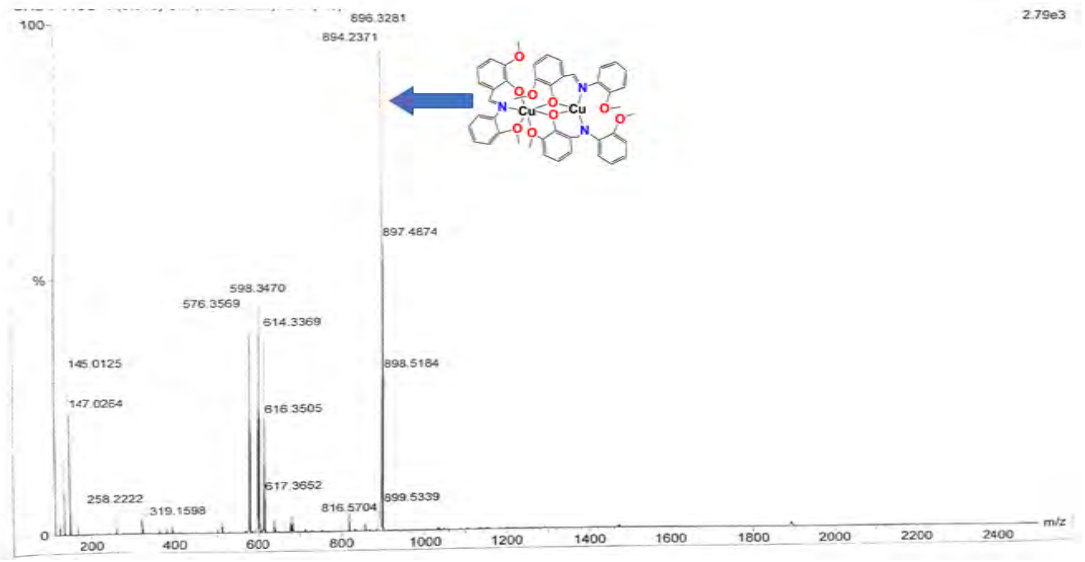

Fig. 5.7. ESI-Ms spectrum of the complex **4** in MeCN medium

5.3.8. Theoretical calculation of complex 4

To get an idea about the electronic transitions and molecular level reactivity, energy of frontier molecular orbitals of **4** have been computed and presented in **Fig. 5.8**. Electronic charge density of HOMO, HOMO–1 and HOMO–2 were located majorly both on the ligand and metal centres and electronic charge density of LUMO, LUMO+1 and LUMO+2 were exclusively located on the ligand. Besides, the transition energies or energy gap among the frontier molecular orbitals, HOMO-LUMO, (HOMO–1)-(LUMO+1) and (HOMO–2)-(LUMO+2) were calculated as 2.69 eV (525 nm), 3.42 eV (473 nm) and 3.95 eV (435 nm) respectively. This transition energy values suggested the molecular level reactivity of the complex **4**.

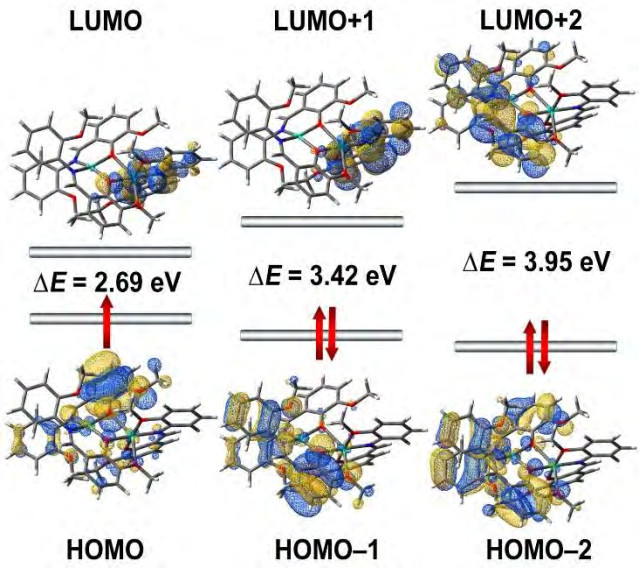

Fig. 5.8. Images of frontier molecular orbitals of binuclear copper complex obtained using DFT/B3LYP/6-311G theoretical method and IEFPCM/MeCN solvent system

5.3.9. Description of crystal structure

X-ray structural analysis exhibited that the complex **4** crystallizes in orthorhombic system with *P*bca space group. Very interestingly, in this complex **4**, each of the copper(II) centres adopted different coordination geometry–octahedral and square planar geometries. An ellipsoidal diagram of **4** was shown in **Fig. 5.9**. The structural refinement parameter for this complex **4** was specified in **Table 5.4**.

Table 5.4. Crystallographic data and structure refinement parameters for **4**

Parameters	**4**
CCDC Number	1957033
Empirical formula	$C_{45}H_{42}N_3O_{13}C1Cu_2$
Formula weight	995.34
Temperature (K)	100
Crystal system	Orthorhombic
Space group	*P*bca
a (Å)	20.6993(10)
b (Å)	15.1138(9)
c (Å)	26.913(2)
Volume ($Å^3$)	8419.6(9)

Z	8
ρ (gcm^{-3})	1.571
μ (mm^{-1})	1.146
Temperature (K)	100
F (000)	4096
R_{int}	0.088
θ ranges (º)	2.5-25.0
Number of unique reflections	7402
Total number of reflections	40939
Final R indices	0.0685, 0.2393
Largest peak and hole ($eA^{\circ -3}$)	1.19, -1.24

Weighting Scheme: $R= \Sigma|Fo|-|Fc||/\Sigma|Fo$, $wR2=[\Sigma w(Fo^2-Fc^2)^2/\Sigma w(Fo^2)^2]^{1/2}$, Calc. $w = 1/[\sigma^2(Fo^2) + (0.1260P)^2+ 18.6138P]$ (**4**); where $P = (Fo^2+2Fc^2)/3$.

The bond angles as well as bond distances were given in **Table 5.5**. Three units of $\mathbf{L^4}$ in coupling with two Cu(II) ions produce a monocationic complex **4** and the cationic charge was satisfied by perchlorate ion in the secondary zone of coordination. $\mathbf{L^4}$ may be considered as a tetradentate chelator for consisting of four donor centres in its structure although it only coordinates using three donor centres and behaves as a flexidentate ligand system. The square planar geometry for Cu1 centre in **4** deviated slightly from ideal square planar geometry and it was evident from the measurements of bond angles (**Table 5.5**).[53,54] The origin of distorted square planar geometry may be assigned to the presence of bond constraints in Schiff base ligand during coordination to copper ion. The Cu2 centre in **4** adopted a distorted octahedral geometry. The equatorial plane of the octahedron was effectively formed by the donor groups (O1, O2, N3, O4) those were closer to the Cu(II) center while the two oxygen atoms (O3,O8) were placed at longer distance giving a distorted octahedron (**Fig.5.9**). This tetragonally flattened octahedral geometry of Cu2 centre about Z axis with two shorter and four longer bonds was caused by Jahn-Teller distortion and formally called as Z_{in} distortion.[55] Cu1 and Cu2 centres in the complex **4** were interconnected by $\mu_{1,1}$-type phenoxo bridges with a separation distance of 3.182 Å.

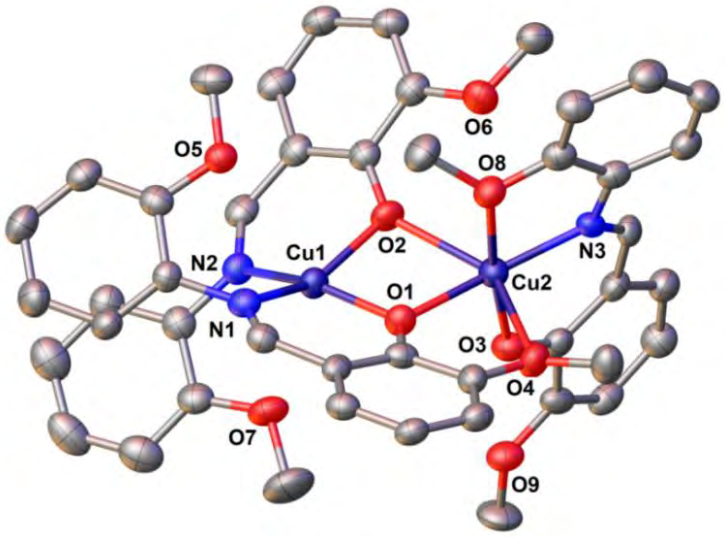

Fig. 5.9. An ORTEP plot of complex **4** with 30% ellipsoid probability (H atoms are removed to enhance clarity)

Table 5.5. Bond distances and bond angles for the complex **4**

Bond lengths (Å)					
	XRD	DFT		XRD	DFT
Cu1-O1	1.931(4)	1.952	Cu2-O1	2.010(4)	1.968
Cu1-O2	1.931(4)	1.958	Cu2-O2	2.340(4)	2.406
Cu1-N1	1.991(5)	1.996	Cu2-O3	1.903(5)	1.955
Cu1-N2	1.970(5)	1.980	Cu2-O4	2.425(4)	2.377
			Cu2-O8	2.083(5)	2.035
			Cu2-N3	1.939(5)	1.966
Bond angles (˚)					
O1-Cu1-O2	83.52(18)	82.64	O1-Cu2-O3	95.96(18)	94.98
O1-Cu1-O5	123.35(16)	117.16	O1-Cu2-O4	72.17(15)	74.51
O1-Cu1-O7	96.57(17)	92.61	O1-Cu2-O8	88.58(17)	91.05
O1-Cu1-N1	92.18(18)	91.22	O1-Cu2-N3	166.27(18)	170.36
O1-Cu1-N2	161.37(19)	155.88	O2-Cu2-O3	96.23(17)	83.17
O2-Cu1-O5	92.24(16)	92.29	O2-Cu2-O4	144.03(14)	145.33
O2-Cu1-O7	128.50(17)	123.01	O2-Cu2-O8	89.50(16)	95.70
O2-Cu1-N1	147.02(19)	152.44	O2-Cu2-N3	116.97(17)	115.57
O2-Cu1-N2	94.58(19)	92.74	O3-Cu2-O4	90.94(17)	93.02
O5-Cu1-O7	127.14(14)	138.85	O3-Cu2-O8	173.57(17)	173.15
O5-Cu1-N1	63.04(15)	68.64	O3-Cu2-N3	93.33(18)	92.44
O5-Cu1-N2	75.17(16)	86.40	O4-Cu2-O8	86.10(16)	91.73
O7-Cu1-N1	84.45(17)	83.96	O4-Cu2-N3	97.64(16)	98.98
O7-Cu1-N2	70.11(17)	70.05	O8-Cu2-N3	81.43(17)	81.94
N1-Cu1-N2	99.2(2)	103.01	Cu1-O1-Cu2	107.66(19)	109.46
O1-Cu2-O2	72.04(16)	71.55	Cu1-O2 -Cu2	95.82(17)	93.77

The complex **4** was optimized in vacuum for ground state employing unrestricted density functional theory (DFT) and optimized structure was shown in **Fig. 5.10**. The DFT optimized structure was correlated with XRD structure to reveal the degree of similarity in structural connectivity and coordination geometries of copper(II) centres. The DFT computed geometrical parameters for the complex **4** were listed in **Table 5.5**. These bond length and bond angle data exactly reproduced the XRD data. These observations provide additional support in favour of the geometrical orientation of the ligand around the metal centres. Additionally, superimposition of the XRD structure (orange, **Fig. 5.11**) with DFT optimized structure (violet, **Fig. 5.11**) was performed using PyMOL 1.3 software. The DFT optimized structure exactly reproduced the XRD structure which stands with the diverse coordination motif of Cu(II) at two different position within **4**. The crystal structure exhibited same degree of coordination linkages between Cu(II) and $\mathbf{L^4}$ and coordination geometries of each of the copper(II) centres in complex **4**.

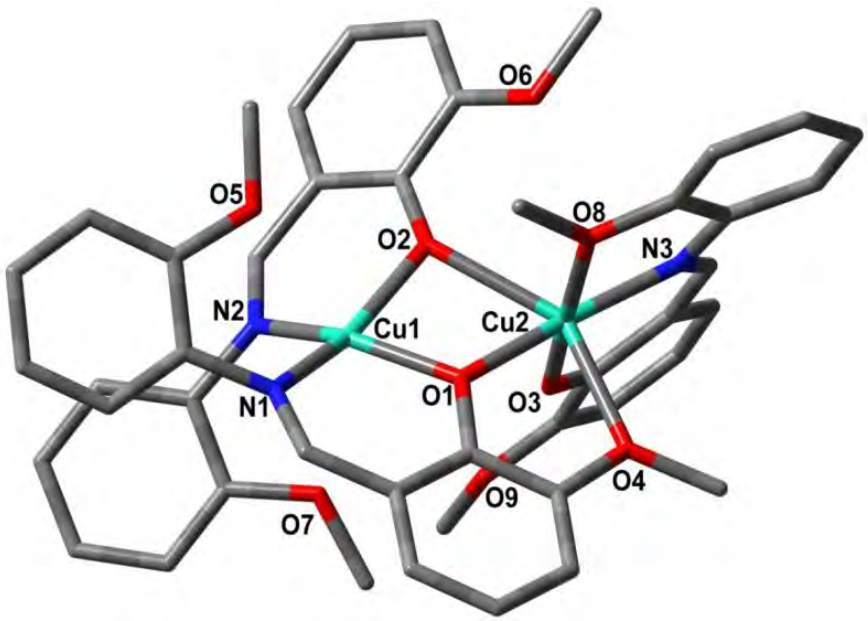

Fig. 5.10. Optimized structure of **4** in vacuum employing DFT/B3LYP/6-311G theoretical model

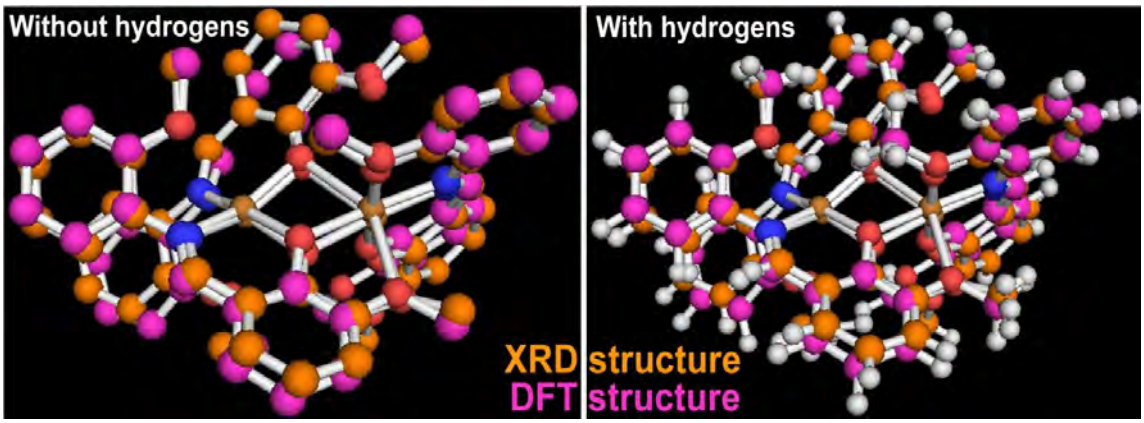

Fig. 5.11. XRD structure and DFT structure superimposed with each other using PyMOL 1.3. software

5.3.10. Hirshfeld analysis of complex 4

Hirshfeld surface of Cu(II) complex (**Fig. 5.12**) over a definite d_{norm} has been calculated using Crystal Explorer software. The calculated surface volume was found as 963.85 $Å^3$ and surface area was determined as 687.91 $Å^2$. The red highlighted area showed the d_{norm} area and close non-covalent interactions of **4** with its surrounding analog within the 3D crystal. Percentage share of each element in close interaction with others was given in **Table 5.5**. In this d_{norm}, the blue area was showing the weak π···π interactions between aromatic rings of the ligands and most of area remains white which means there was no interaction. Red area presents weak C-H···O H-bonding between C-H of benzene ring and O of ClO_4. This molecule was interacted by surrounding molecules through C-H···O hydrogen bond, C-H···π and π···π interactions as display in Fingerprint plots (**Fig. 5.13**). Quantitative information of different intermolecular interactions by each pair of elements was given in **Table 5.6**. In the fingerprint plot, the direction of interaction was towards weak interactions employing hydrogen atoms (inside and outside of hirshfeld surface centre peak) and carbon atoms of C-H···π interactions.

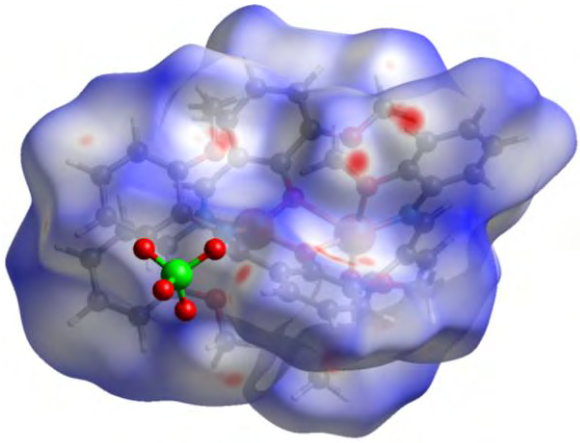

Fig. 5.12. Hirshfeld surface of complex **4**

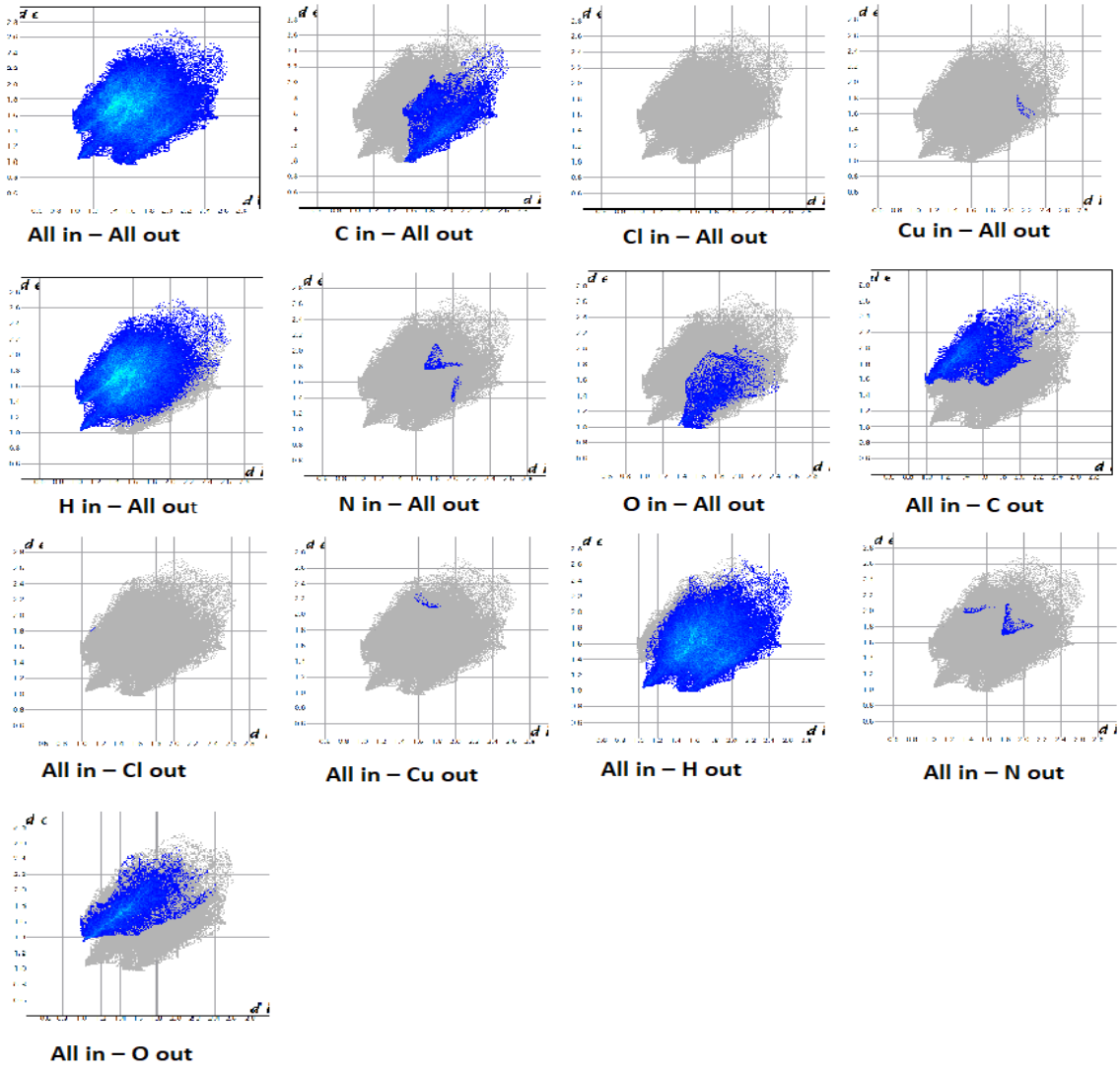

Fig.5.13. Fingerprint plot of complex **4**

Table 5.6. Percentage share of the interaction of each atom with other atoms when they were in or out of the Hirshfeld surface

Atom inside the surface	Atom outside the surface	% Contributing in interaction
Cu	All	0.1
Cl	All	0.0
O	All	4.9
N	All	0.4
C	All	16.0
H	All	78.7
All	Cu	0.1
All	Cl	0.0
All	O	17.0
All	N	0.4
All	C	14.2
All	H	68.3

5.3.11. Phenoxazinone synthase mimicking activity of the complex 4

The 2-aminophenol oxidation activity by the complex **4** was examined using a model substrate 2-aminophenol (2-AP) under the aerobic condition in MeCN at room temperature (25°C) (**Scheme 5.3**).

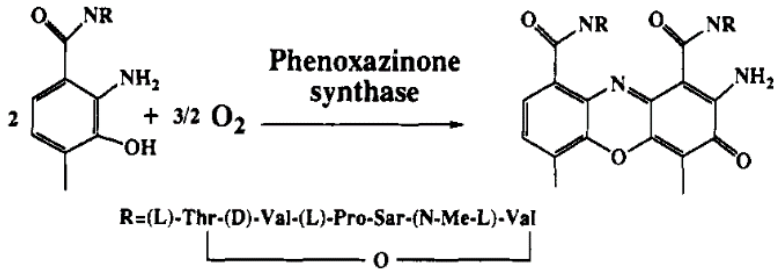

Scheme 5.3. Catalytic oxidation of 2-aminophenol by phenoxazinone synthase

To study the catalytic oxidation of 2-aminophenol, 1×10^{-4} M solution of Cu(II) complex was added to a 1×10^{-3} M solution of 2-AP in MeCN medium. The course of catalysis was monitored using UV–Vis spectrophotometer. The time-dependent scan was recorded at a time interval of 5 min for 2h (**Fig. 5.14**). 2-AP in MeCN solution displays a single band at 267 nm which was an indication for its pure form in solution. On addition of complex **4** to 2-AP in MeCN, a new band at 434 nm with incremental absorbance was observed (**Fig. 5.14**) and concomitantly, solution in cuvette starts to

turn brown. Appearance of this new electronic band at 434 nm in presence of complex **4** was a pure signature for the production of aminophenoxazinone species in MeCN.[6,42,79]

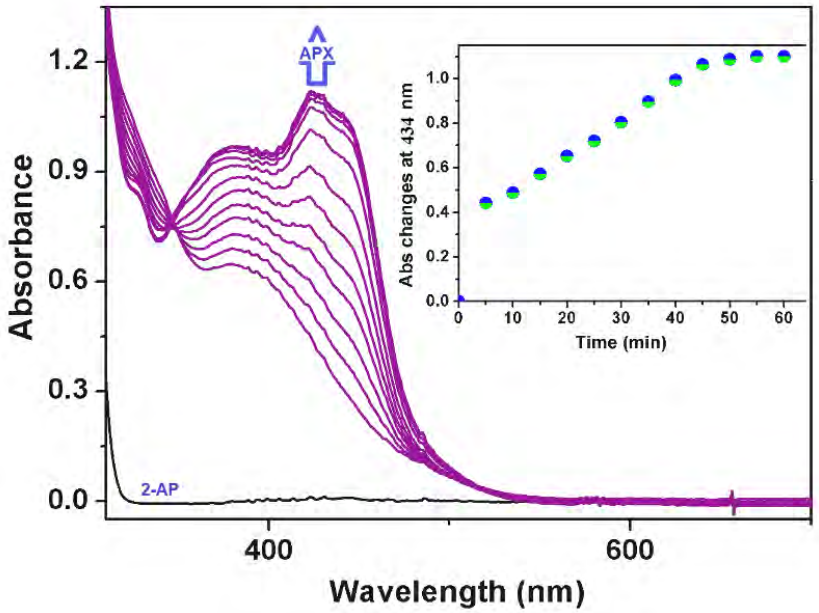

Fig. 5.14. Rise of optical band at 434 nm for the growth of APX in solution upon addition of complex **4** to 100 equivalents of 2-AP in acetonitrile medium. (The spectra are recorded after every 5 min). Inset: Time vs Absorbance plot at defined wavelength

The controlled experiment was also carried out to find out the role of Schiff base in this phenoxazinone synthase mimicking activity using 2-AP in MeCN solvent under the aerobic atmosphere at room temperature. Controlled experiment was also carried out using catalytic amount of Schiff base in 2-AP under identical reaction conditions (**Fig. 5.15**). Although, no considerable amount of growth for phenpxazinone species is noted up to 3h. The titration curves got saturated after 1h of catalysis by the complex **4**.

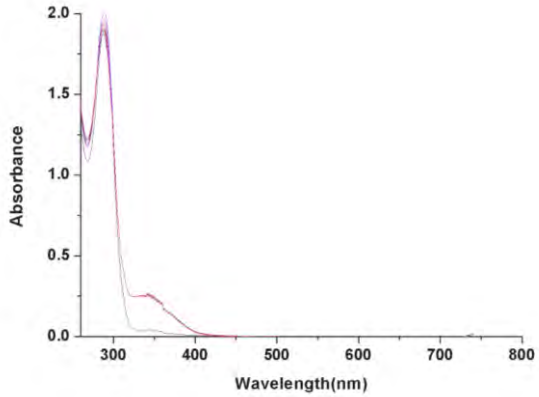

Fig. 5.15. Controlled experiment using catalytic amount of Schiff base in 2-AP under identical reaction conditions

The details of kinetic investigations for the catalytic oxidation of 2-AP were performed to realize the efficacy for this copper(II) catalyst. The method of initial rates was followed to unveil the nature of kinetic for this catalytic oxidation of 2-AP. The growth of phenoxazinone species was monitored at 434 nm as a function of time (**Fig. 5.16.**).[6,32,42,56,57,58,59] The plot of rate constants versus concentration of the substrate displays the saturation kinetics (**Fig. 5.16.**) where Michaelis−Menten equation looks to be appropriate (**Fig. 5.16.**). The catalyst–substrate adduct (CS) that decomposes in a second step to release free catalyst (C) and product (P) was represented below.

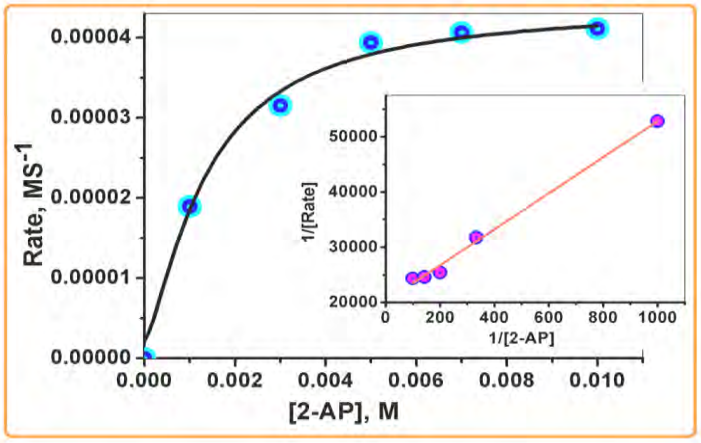

Fig. 5.16. Plot of Rate of reaction vs [2-AP] for the catalytic oxidation of 2-AP by complex **4** in acetonitrile

Table 5.7. Comparison of k_{cat} (h^{-1}) values for catalytic oxidation of 2-AP by reported copper complexes and **4**

Complex	k_{cat} (h^{-1})(Solvent)	CCDC No	Ref
$[L^1Cu(\mu\text{-}Cl)_2CuL^1]$	1065 (CH_3OH) 213 (CH3CN)	1572023	[80]
$[Cu_4(L^2)_4]$	86.3 (CH_3OH)	1507035	[81]
$[Cu_4(L^3)_4]$	340.26 (CH_3OH)	1507036	[81]
$[Cu_4(L^4)_4]$	1.21×10^5(CH_3OH)	1455999	[82]
[Cu(μ-Cl)(Phen)Cl]	1.69×10^4(CH_3OH)	1524680	[6]
$[(CH_3CN)Cu(L_s)_2Cu]^{2+}$	11.1 (CH_3OH)	1940162	[83]
$[Cu_2(L)_3]ClO_4$	78.14 (CH_3OH)	1957033	This work

L^1 = 2-(a-Hydroxyethyl)benzimidazole (Hhebmz), L^2 = (E)-4-Chloro-2-((thiazol-2-ylimino)methyl)phenol, L^3 = (E)-4-Bromo-2-((thiazol-2-ylimino)methyl)phenol, L^4 = N-(2-hydroxyethyl)-3-methoxysalicylaldimine.

The Michaelis–Menten equation may be written as:

$$V = \frac{V_{max}\,[S]}{K_M + [S]}$$

Where, V was the reaction velocity (the reaction rate), K_m was the Michaelis–Menten constant, V_{max} was the maximum reaction velocity, and [S] was the substrate concentration.

The values of kinetics parameters were determined from Michaelis−Menten approach of enzymatic kinetics **4** as $V_{max}(MS^{-1}) = 2.17\times10^{-6}$; $K_M = 4.40\times10^{-4}$ [Std. Error for V_{max} $(MS^{-1}) = 1.17\times10^{-7}$; Std. Error for K_m (M)= 1.40×10^{-5}].

A comparison of phenoxazinone synthase reactivity was drawn between this complex **4** and some other reported copper(II) and presented in **Table 5.7**.[80-83] The catalytic efficiency for **4**, $k_{cat}/K_M = 1.77\times10^5$ towards catalytic aminophenol oxidation was also encountered as high.

Electrochemical and electron paramagnetic resonance (EPR) analysis were also carried out to cope the catalytic efficiency of the complex **4** towards the catalytic oxidation of 2-AP in acetonitrile medium. The electrochemical behavior was recorded in dichloromethane medium at 298 K using cyclic voltammetry. N-tetrabutylammonium hexafluorophosphate was used to record the electrochemical data under aerobic condition and presented in **Fig. 5.17**. The electrochemical data in reference with ferrocenium/ferrocene (Fc+/Fc) couple were summarized in **Table 5.8**. This complex **4** exhibited one irreversible cathodic wave at -1.40 V which was assignable to electron transfer in Cu^{2+} to Cu^{+} redox couple in solution phase. Another irreversible peak was appeared at 0.0095 V which may probable for the deposition of Cu. The active participation of copper(II) centre in catalytic oxidation of 2-AP was confirmed by measurement of redox potentials of Cu(II) complex in presence of 2-AP under identical reaction conditions. The mixture of complex **4** in presence of 2-AP produces irreversible anodic peak at 0.134 V which strongly suggest the oxidation of 2-aminophenol to iminoquinone (**Fig. 5.17**). To view more insights of this complex **4** mediated oxidative coupling of 2-AP, EPR spectra of the Cu(II) complex in presence and absence of 2-AP are recorded in MeCN medium. The EPR spectrum of complex **4** with X-band frequency at room temperature in MeCN medium displayed silent nature of spectral profile and suggests the possibility of phenoxo-bridged magnetically coupled copper(II) centres through antiferromagnetic interactions. Bond angle measurements

[∠Cu2-O1-Cu1, 107.66°; ∠Cu2-O2-Cu1, 95.82°] and literature reviews recommend further about the dominance of antiferromagnetic interactions between the copper(II) centres. [15-24]

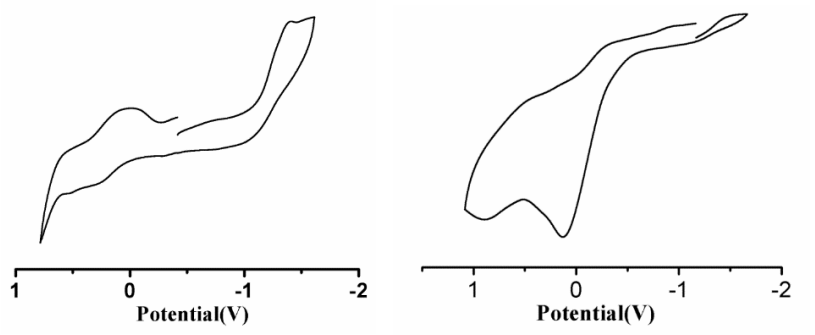

Fig. 5.17. Left: Cyclic voltammogram of the complex **4** in anhydrous DCM medium; **Right:** Cyclic voltammogram of the mixture of complex **4** and 2-AP under molecular oxygen atmosphere in anhydrous DCM in CH_2Cl_2 (0.20 M $[N(n-Bu)_4]PF_6$) at 295 K

Table 5.8. Redox potentials data of complex **4** in presence and absence of 2-AP referenced to Fc+/Fc couples determined by cyclic voltammetry in CH_2Cl_2 (0.20 M $[N(n-Bu)_4]PF_6$) at 295 K

Compounds	$E_{1/2}{}^1$ (V) (ΔE^a, mV)	$E_{½}{}^2$,V (ΔE^a, mV)
Metal Complex		-1.4V, 0.0095 V
Metal Complex+ 2AP	0.134 V	
[a]peak to peak separation in mV, [b]anodic peak, [c]cathodic peak		

The EPR spectral analysis of the copper complex in presence of 2-AP in acetonitrile medium at room temperature strongly suggested the generation of radical species for the appearance of additional signal at g ca 2.057 (**Fig. 5.18**). The reported g value for oxidised 2-AP radical (iminobenzoquinone) was 2.0051 in 10^{-1} M Bu_4NPF_6.[6,10,42]

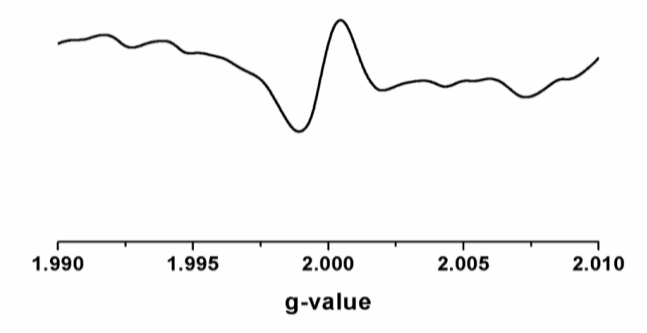

Fig. 5.18. X- band EPR spectra of the complex **4** in presence of 2-AP after 20 min in CH_3CN solution at 298 K

Furthermore, electrospray ionization (ESI) mass spectrum of the complex **4** in presence of 2-AP was recorded after mixing of 15 mins to reveal the binding aspects of the complex **4** and 2-AP in MeCN medium. It was observed that the ESI-Ms of the reaction mixture (**Fig. 5.19**) exhibited the base peak at m/z 214.56 which was attributed to the existence of aminophenoxazinone compound, [(2-amino-3*H*-phenoxazine-3-ones)+H^+] in the solution. Furthermore, another characteristics peak at m/z 1004.6951 was defined as the binding adduct between complex **4** and 2-AP, [[**4**+(2-AP)]+H^+]. It was supposed to consider that square planar copper centre facilitates the formation of adduct with 2-AP for its existence in less hindered coordinative environment. In this context, to view the chemical fate of molecular oxygen during the course of phenoxazinone mimics activity, the production of hydrogen peroxide has been examined following a reported procedure. [56-59] The production of hydrogen peroxide (**Fig. 5.20**) has been detected through rise of spectral band at λ_{max} 353 nm and this observation justifies the active involvement of molecular oxygen in this course of catalysis.

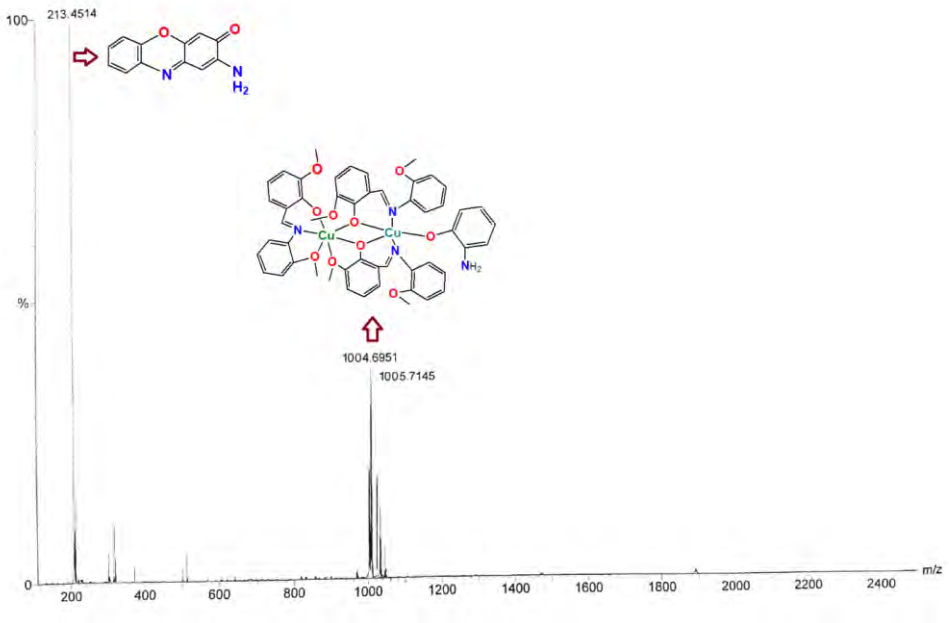

Fig. 5.19. ESI-Ms spectrum of the complex **4** in presence of 2-AP in MeCN medium

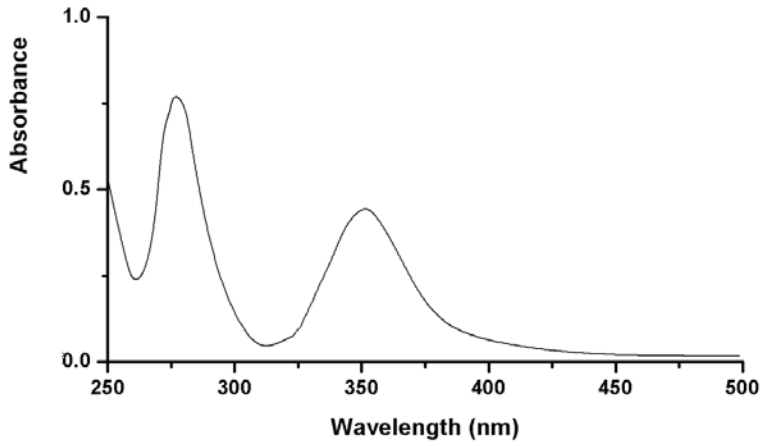

Fig. 5.20. Absorbance profile of I_3^-

Previously studied by P. Chaudhury and co-workers [84] about the bio-mimicking activities of the oxidation of 2-AP involving tetracopper complex strongly recommends and accounts on an "on-off" mechanism mediated via radical generation in active participation with the metal centers favouring 6e oxidative coupling of substrate. Another renowned scientist, T.P. Begley *etal.*[85-87] suggested the production of 2-aminophenoxazinone through a sequence of three consecutive 2e oxidation of 2-AP. The tautomerization reactions were the controlling unit in regeneration of the 2-Ap during this course of catalytic oxidation reaction.

Based upon important spectroscopic and electro-analytical methods, it may be proposed that the oxidation coupling of 2-AP (**Scheme. 5.4**) undergoes through formation of catalyst-substrate intermediate (B1) in the primary stage. Later on, the Cu2 centre activated molecular oxygen (C) leading to production of hydrogen peroxide and iminobenzoquinone in the course of catalytic oxidation. Iminobenzoquinone undergoes coupling with another 2-AP and leads to aminophenoxazinone species.

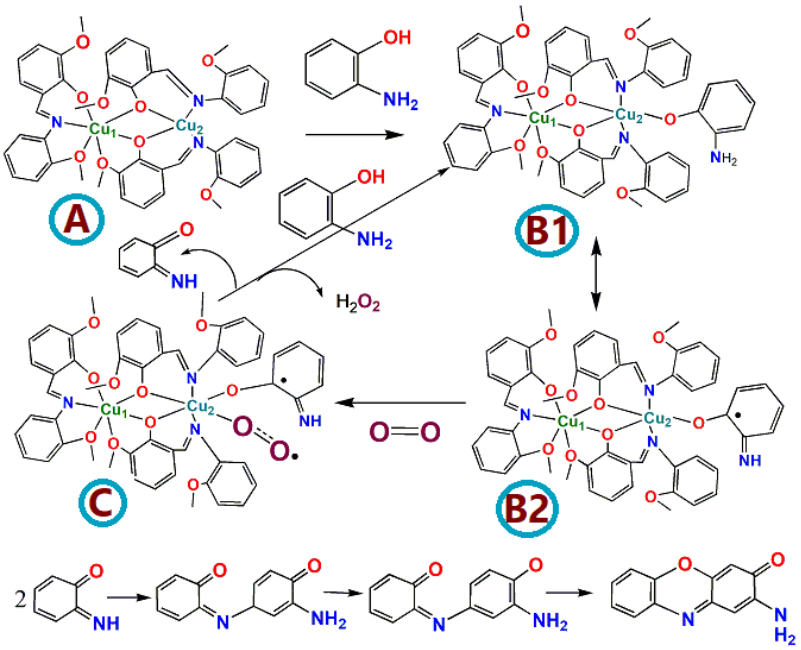

Scheme. 5.4. Plausible mechanistic pathways for the catalytic oxidative coupling of 2-AP by complex **4**

To correlate the experimental observation, ground state geometries of both the **B1** and **B2** molecular adducts were optimized computationally and presented in **Fig. 5.21**. The potential energy of **B2** was found to be slightly higher (E = – 6223.82988265 au) than **B1** (E = – 6224.43218979 au). The theoretical calculation strongly supports the formation of enzyme-substrate adducts (**B1** and **B2**) and denoted that **B1** might easily be converted into **B2** by prevailing over slight potential energy difference. Therefore, it could be stated that **A** interacts with aminophenol to form **B1** which might be converted into **B2**. Then, **B2** might interact with molecular oxygen to form **C**. Hence, computational calculation moderately supports the plausible catalytic pathways in the oxidative coupling of 2-AP (**Scheme 5.4**).

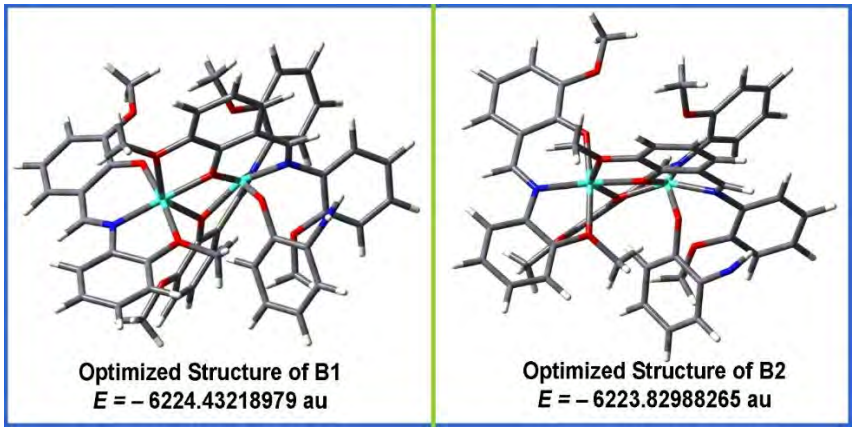

Fig. 5.21. Ground state optimized geometries of **B1** and **B2** with corresponding potential energy values employing DFT/B3LYP/6-311G theoretical method

5.4. Conclusions

A new dinuclear copper(II) complex, $[Cu_2(\mathbf{L^4})_3]ClO_4$ (**4**) has been developed based on a Schiff base ligand,. The structural geometry of the dicopper(II) compound was confirmed principally by single crystal X-ray diffraction study with routine analytical techniques. The copper(II) complex crystallizes in orthorhombic system with *P*bca space group. X-ray structure of **4** revealed that $\mathbf{L^4}$ behaves as a tridentate chelator towards Cu(II) ion during chelation although $\mathbf{L^4}$ was actually a tetradentate chelating ligand. Moreover, three Schiff base units with two Cu(II) ions build a dinuclear copper(II) complex through phenoxido bridges of Schiff base ligands. Interestingly, two Cu(II) centres in **4** adopted hetero-geometries (octahedral and square pyramidal) in **4**. Evaluation of bio-mimetic efficiency of the Cu(II) compound towards 2-aminophenol (2-AP) as a model substrate in acetonitrile medium, it was observed that this Cu(II) complex catalyzes the oxidative coupling of 2-AP to aminophenoxazinone species with a significant turnover number, 78.14 h^{-1}. EPR, cyclic voltagram and ESI-MS strongly suggested the formation of enzyme-substrate adduct which subsequently produces iminibenzoquinone and the course of bio-oxidative catalysis undergoes through radical species along with the development of aminophenoxazinone species and hydrogen peroxide as products. Theoretical calculations employing DFT supports the structural aspects and observed reaction pathways of phenoxazinone synthase activity of the copper complex very well. This compound represents an example where two hetero-geometric copper(II) centres were co-existed through phenoxo bridged. Magnetic aspect will be investigated in future and this compound may be a suitable candidate to exhibited potential biological activity.

References

[1]. P.G. Cozzi, *Chem. Soc. Rev*., 2004, **33**, 410-421.

[2]. A. S. Smirnov, L. M. D. R. S. Martins, D. N. Nikolaev, R.A. Manzhos, V. V. Gurzhiy, A. G. Krivenko, K. O. Nikolaenko, A.V. Belyakov, A.V. Garabadzhiua and P. B. Davidovich, *New J. Chem*., 2019, **43**, 188.

[3]. W. A. Zoubi and Y. G. Ko, *Appl. Organomett. Chem*., 2017, **31**, e3574.

[4]. E. I. Solomon, D. E. Heppner, E. M. Johnston, J. W. Ginsbach, J. Cirera, M. Qayyum, M. T. Kieber-Emmons, C. H. Kjaergaard, R. G. Hadt and L. Tian, *Chem. Rev*., 2014, **114**, 3659–3853.

[5]. E. I. Solomon, M. J. Baldwin and M. D. Lowery, *Chem. Rev*., 1992, ***92***, 521-542.

[6]. M. Garai, D. Dey, H. R. Yadav, A. R. Choudhury, M. Maji and B. Biswas, *ChemistrySelect*, 2017, **2**, 11040-11047.

[7]. C. Mukherjee, U. Pieper, E. Bothe, V. Bachler, E. Bill, T. Weyhermu¨ller and P. Chaudhuri, *Inorg. Chem*., 2008, **47**, 8943–8956.

[8]. P. Chakraborty , J. Adhikary , B. Ghosh, R. Sanyal, S. K. Chattopadhyay , A. Bauzá , A. Frontera , E. Zangrando and D. Das , *Inorg. Chem*., 2014, **53**, 8257-8269.

[9]. G.C. Paul, K. Das, S. Maity, S. Begum, H. K. Srivastava and C. Mukherjee, *Inorg. Chem*., 2019, **58**, 1782-1793.

[10]. P. Mahapatra, S. Ghosh, S. Giri, V. Rane, R. Kadam, M. G. B. Drew and A. Ghosh, *Inorg. Chem*., 2017, **56**, 5105-5121.

[11]. K. D. Karlin, Z. Tyekla`r, A. Farooq, M. S. Haka, P. Ghosh, R. W. Cruse, Y. Gultneh, J. C. Hayes, P. J. Toscano and J. Zubieta, *Inorg. Chem*., 1991, **31**, 1436–1451.

[12]. E. I. Solomon, R. K. Szilagyi, S. DeBeer George and L. Basumallick, *Chem. Rev*., 2004, **104**, 419–458.

[13]. D. J. Spira- Solomon, M. D. Allendorf and E. I. Solomon, *J. Am. Chem. Soc*., 1986, **108**, 5318–5328.

[14]. E. I. Solomon, U. M. Sundaram and T. E. Machonkin, *Chem. Rev*., 1996, **96**, 2563–2605.

[15]. T. Mallah, O. Kahn, J. Gouteron, S. Jeannin, Y. Jeannin and C. J. O'Connor, *Inorg. Chem*., 1987, **26**, 1375–1380.

[16]. A. Benzekri, P. Dubourdeaux, J.-M. Latour, P. Rey and J. Laugierb, J. Chem. Soc., Dalton Trans., 1991, 3359–3365.

[17]. A. Benzekri, P. Dubourdeaux, J.-M. Latour, J. Laugier and P. Rey, *Inorg. Chem*., 1988, **27**, 3710–3716.

[18]. A. Banerjee, R. Singh, E. Colacio and K. K. Rajak, *Eur. J. Inorg. Chem*., 2009, 277–284.

[19]. P. Cheng, D. Liao, S. Yan, Z. Jiang, G. Wang, X. Yao and H. Wang, *Inorg. Chim. Acta*., 1996, **248**, 135–137.

[20]. P. Bhowmik, A. Bhattacharyya, K. Harms, S. Sproules and S. Chattopadhyay, *Polyhedron*, 2015, **85**, 221–231.

[21]. A. Biswas, M. G. B. Drew, J. Ribas, C. Diaz and A. Ghosh, *Eur. J. Inorg. Chem*., 2011, 2405–2412.

[22]. S. S. Massoud, C. C. Ledet, T. Junk, S. Bosch, P. Comba, R. Herchel, J. Hosˇek, Z. Tra´vnı´cˇek, R. C. Fischer and F. A. Mautner, *Dalton Trans*., 2016, **45**, 12933–12950.

[23]. S. S. Massoud, A. A. Gallo, M. J. Dartez, J. G. Gautreaux, R. Vicente, J. H. Albering and F. A. Mautner, *Inorg. Chem. Commun*., 2014, **43**, 35–38.

[24]. S. S. Massoud, T. Junk and F. A. Mautner, *RSC Adv*., 2015, **5**, 87139–87150.

[25]. S. Cao, R. Cheng, D. Wang, Y. Zhao, R. Tang, X. Yang and, J. Chen, *J. Inorg. Biochem*., 2019, **192**, 126-139.

[26]. P. Kar, A. Franconetti, A. Frontera and A. Ghosh, *Cryst. Eng. Comm*., 2019, **21**, 6886-6893.

[27]. A. Shirvan, H. Golchoubian and E. Bouwman, J. Mol. Struct., 2019, **1195**, 769-777.

[28]. A. Hussain, M. F. AlAjmi, M. T. Rehman, S. Amir, F. M. Husain, A. Alsalme, M. A. Siddiqui, A. A. AlKhedhairy and R. A. Khan, *Scientific Reports*., 2019, **9**, 5237.

[29]. Y.-X. Sun, Y.-Q. Pan, X. Xu and Y. Zhang, *Crystals*, 2019, **9**, 607.

[30]. J. McLain, J. Lee and J. T. Groves, Biomimetic Oxidations Catalyzed by Transition Metal Complexes, In: Meunier, B. (Ed.), Imperial College Press, London,

[31]. F. Benedini, G. Galliani, M. Nali, B. Rindone and S. Tollari, *J. Chem. Soc. Perkin Trans*., 1985, **2,** 1963.

[32]. L. I. Simandi, S. Nemeth and N. Rumlis, *J. Mol. Catal*., 1987, **42**, 357.

[33]. Z. Szeverenyl, E. R. Mileava, L. I. Simandi, *J. Mol. Catal*., 1991, **67**, 251.

[34]. S. Roy, T. Dutta, M. G. B. Drew and S. Chattopadhyay, *Polyhedron*, 2019

doi.org/10.1016/j.poly.2019.114311.

[35]. N. C. Jana, M. Patra, P. Brandão and A. Panja, *Inorg. Chim. Acta*., 2019, **490**, 163-172.

[36]. K. Ghosh, M. G. B. Drew and S. Chattopadhyay, *Inorg. Chim. Acta*., 2018, **482**, 23-33.

[37]. S. Thakur, S. Banerjee, S. Das and S. Chattopadhyay, *New J. Chem*., 2019, **43**, 18747-18759.

[38]. S. Sakaue, T. Tsubakino, Y. Nishiyama and Y. Ishii, *J. Org. Chem*., 1993, **58**, 3633.

[39]. J. Kaizer, R. Csonka and G. Speier, J. Mol. *Catal. A: Chem*., 2002, **180**, 91.

[40]. T. Horvath, J. Kaizer and G. Speier, *J. Mol. Catal. A: Chem*., 2004, **215**, 9.

[41]. M. R. Maurya, S. Sikarwar, T. Joseph and S. B. Halligudi, *J. Mol. Catal. A: Chem*., 2005, **236**, 132.

[42]. M. Garai, A. Das, M. Joshi, S. Paul, M. Shit, A. R. Choudhury and B. Biswas, *Polyhedron*, 2018, **156**, 223-230.

[43]. D. Dey, G. Kaur, A. Ranjani, L. Gayathri, P. Chakraborty, J. Adhikary, J. Pasan, D. Dhanasekaran, A. R. Choudhury, M. A. Akbarsha, N. Kole and B. Biswas, *Eur. J. Inorg. Chem*., 2014, 3350-3358.

[44]. D. Dey, G. Kaur, M. Patra, A. R. Choudhury, N. Kole and B. Biswas, *Inorg. Chim. Acta*., 2014, **421**, 335-341.

[45]. CrysAlisPro 1.171.39.35c, 2017, Rigaku Oxford Diffraction, Rigaku Corporation: Tokyo, Japan.

[46]. G. M. Sheldrick, *Acta Cryst*., 2015, **A71**, 3-8.

[47]. G. M. Sheldrick, *Acta Cryst*., **2015**, *C71*, 3-8.

[48]. O. V. Dolomanov, L. J. Bourhis, R. J. Gildea, J. A. K. Howard and H. Puschmann, *J. Appl. Cryst*., 2009, **42**, 339-341.

[49]. M. J. Turner, J. J. McKinnon, S. K. Wolff, D. J. Grimwood, P. R. Spackman, D. Jayatilaka and M. A. Spackman, *Crystal Explorer*, http://hirshfeldsurface.net17, 2017.

[50]. M. A. Spackman and D. Jayatilaka, *CrystEngCom*., 2009, **11**, 19.

[51]. S. K. Seth, V. S. Lee, J. Yana, S. M. Zain, A. C. Cunha, V. F. Ferreira, A. K. Jordao, M. C. B. V. de Souza, S. M. S. V. Wardell, J. L. Wardellf and E. R. T. Tiekink, *Cryst. Eng. Comm*., 2015, **17**, 2255-2266.

[52]. M. N. Ahamad, M. Kumar, A. Ansari, I. Mantasha, M. Ahmad and M. Shahid, *New J. Chem*., 2019, **43**, 14074-14083.

[53]. M. A. Spackman and D. Jayatilaka, *Cryst. Eng. Comm*., 2009, **11**, 19-32.

[54]. M. A. Spackman and J. J. McKinnon, *Cryst. Eng. Comm*., 2002, **4**, 378-392.

[55]. H. Yamatera, Acta Chem. Scand. A., 1979, **33**, 107-111.

[56]. C. K. Pal, S. Mahato, H. R. Yadav, M. Shit, A. R. Choudhury, B. Biswas, *Polyhedron*, 2019, **174**, 114156.

[57]. D. Dey, S. Das, H. R. Yadav, A. Ranjani, L. Gyathri, S. Roy, P. S. Guin, D. Dhanasekaran, A. R. Choudhury, M. A. Akbarsha and B. Biswas, *Polyhedron*, 2016, **106**, 106-114.

[58]. A. De, M. Garai, H. R. Yadav, A. R. Choudhury and B. Biswas, 2017, **31**, e3551.

[59]. B. Chowdhury, M. Maji and B. Biswas, *J. Chem. Sci*., 2017, **129**, 1627-1637.

[60]. M. J. Frisch, G. W. Trucks, H. B. Schlegel, G. E. Scuseria, M. A. Robb, J. R. Cheeseman, G. Scalmani, V. Barone, B. Mennucci, G. A. Petersson, H. Nakatsuji, M. Caricato, X. Li, H. P. Hratchian, A. F. Izmaylov, J. Bloino, G. Zheng, J. L. Sonnenberg, M. Hada, M. Ehara, K. Toyota, R. Fukuda, J. Hasegawa, M. Ishida, T. Nakajima, Y. Honda, O. Kitao, H. Nakai, T. Vreven, J. A. Montgomery Jr, J. E. Peralta, F. Ogliaro, M. Bearpark, J. J. Heyd, E. Brothers, K. N. Kudin, V. N. Staroverov, R. Kobayashi, J. Normand, K. Raghavachari, A. Rendell, J. C. Burant, S. S. Iyengar, J. Tomasi, M. Cossi, N. Rega, J. M. Millam, M. Klene, J. E. Knox, J. B. Cross, V. Bakken, C. Adamo, J. Jaramillo, R. Gomperts, R. E. Stratmann, O. Yazyev, A. J. Austin, R. Cammi, C. Pomelli, J. W. Ochterski, R. L. Martin, K. Morokuma, V. G. Zakrzewski, G. A. Voth, P. Salvador, J. J. Dannenberg, S. Dapprich, A. D. Daniels, O. Farkas, J. B. Foresman, J. V. Ortiz, J. Cioslowski and D. J. Fox, Gaussian 09 (Revision A.02), Gaussian Inc., Wallingford, CT, 2009.

[61]. T. H. Dunning and P. J. Hay, in Modern Theoretical Chemistry, ed. H. F. Schaefer, *Plenum*, New York, 1976, 3rd edn,

[62]. B. Mennucci, E. Cances and J. Tomasi, *J. Phys. Chem. B*., 1997, **101**, 10506-10517.

[63]. E. Cances, B. Mennucci and J. Tomasi, *J. Chem. Phys*., 1997, **107**, 3032-3041.

[64]. R. Cammi and J. Tomasi, J. Comput. Chem. 16 (1995) 1449-1458.

[65]. S. Miertus, E. Scrocco and J. Tomasi, *Chem. Phys*., 1981, **55**, 117-129.

[66]. M. Karar, S. Paul, B. Biswas, T. Majumdar and A. Mallick, *Dalton Trans*., 2018, **47**, 7059-7096.

[67]. N. Dutta, S. Haldar, G. Vijaykumar, S. Paul, A. P. Chattopadhyay, L. Carrella and M. Bera, *Inorg. Chem*., 2018, **57**, 10802-10820.

[68]. S. Paul, M. Karar, S. Mitra, S. A. S. Shah, T. Majumdar and A. Mallick, *ChemistrySelect*, 2016, **1**, 5547-5553.

[69]. A. De, A. Sahu, S. Paul, M. Joshi, A. R. Choudhury and B. Biswas, *J. Mol. Struct*., 2018, **1167**, 187-193.

[70]. The PyMOL Molecular Graphics System, Version 1.3. Schrodinger, LLC, Mannheim, Germany.

[71]. B. Chowdhury, M. Karar, S. Paul, M. Joshi, A. R. Choudhury and B. Biswas, *Sens. Actuators B: Chem*., 2018, **276**, 560-566.

[72]. A. De, D. Dey, H. R. Yadav, M. Maji, V. Rane, R. M. kadam, A. R. Choudhury and B. Biswas, *J. Chem. Sci*., 2016, **128**, 1775-1782.

[73]. S. Khan, S. Herrero, R. Gonzalez-Prieto, M. G. B. Drew, S. Banerjee and S. Chattopadhyay, *New J. Chem*., 2018, **42**, 13512.

[74]. T. M. Rajendiran, Transit. *Met. Chem*., 2003, **28**, 447–454.

[75]. W. J. Geary, Coord. *Chem. Rev*., 1971, **7**, 81.

[76]. D. Dey, S. Pal, P. P. Bag, S. Saha, S. Chandraleka, D. Dhanasekaran, N. Kole and B. Biswas, *J. Indian Chem. Soc*., 2015, **92**, 191-202.

[77]. R. V. Rathod, S. Bera, M. Singh and D. Mondal, *RSC Adv*., 2016, **6**, 34608–34615.

[78]. J. R. Lakowicz, doi:10.1007/978-0-387-46312-4, 2006.

[79]. B. Chowdhury, B. Bhowmik, A. sahu, M. Joshi, S. Paul, A. R. Choudhury and B. Biswas, *J. Chem. Sci*., 2018, **130**, 161.

[80]. A. K. Ghosh, A. Ali, Y. Singh, C. S. Purohit and R. Ghosh, *Inorg. Chim. Acta*., 2018, **474**, 156–163.

[81]. S. Sagar, S. Sengupta, A. J. Mota, S. K. Chattopadhyay, A. E. Ferao, E. Riviere, W. Lewis and S. Naskar, *Dalton Trans*., 2017, **46**, 1249–1259.

[82]. M. Mitra, T. Y. Kundu, G. Kaur, G. Sharma, A. R. Choudhury, Y. Singhd and R. Ghosh, *RSC Adv*., 2016, **6**, 58831–58838.

[83]. T. Dutta, S. Mirdya, P. Giri and S. Chattopadhyay, *Polyhedron*, 2020, **175**, 114164.

[84]. C. Mukherjee, T. Weyhermueller, E. Bothe, E. Rentschler and P. Chaudhuri, *Inorg. Chem*., 2007, **46**, 9895–9905.

[85]. C. E. Barry III, P. G. Nayar and T. P. Begley, *Biochemistry*, 1989, **28**, 6323–6333.

[86]. C. E. Barry III, P. G. Nayar and T. P. Begley, *J. Am. Chem. Soc*., 1988, **110**, 3333–3334.

[87]. J. C. Freeman, P. G. Nayar, T. P. Begley and J. J. Villafranca, *Biochemistry*, 1993, **32**, 4826–4830.